Bone Reports 14 (2021) 101013

Contents lists available at ScienceDirect

Bone Reports

journal homepage: www.elsevier.com/locate/bonr

miR-146a-5p targets *Sirt1* to regulate bone mass

Mingxia Zheng [a,1], Junlong Tan [a,1], Xiangning Liu [a,1], Fujun Jin [a,b], Renfa Lai [a,*], Xiaogang Wang [a,b,**]

[a] *Clinical Research Platform for Interdiscipline of Stomatology, The First Affiliated Hospital of Jinan University & Department of Stomatology, College of Stomatology, Jinan University, Guangdong 510632, China*

[b] *Beijing Advanced Innovation Center for Big Data-Based Precision Medicine, School of Biological Science and Medical Engineering, Beihang University, Beijing 100000, China*

ARTICLE INFO

Keywords:
miR-146a-5p
Sirt1
Osteogenesis
Osteoporosis
MicroRNAs

ABSTRACT

MicroRNAs (miRNAs) have been proven to serve as key post-transcriptional regulators, affecting diverse biological processes including osteogenic differentiation and bone formation. Recently, it has been reported that miR-146a-5p affects the activity of both osteoblasts and osteoclasts. However, the target genes of miR-146a-5p in these procedures remain unknown. Here we identify miR-146a-5p as a critical suppressor of osteoblastogenesis and bone formation. We found that miR-146a-5p knockout mice exhibit elevated bone formation and enhanced bone mass *in vivo*. Consistently, we also found that miR-146a-5p inhibited the osteoblast differentiation of bone marrow mesenchymal stem cells (BMSCs) *in vitro*. Importantly, we further demonstrated that miR-146a-5p directly targeted Sirt1 to inhibit osteoblast activity. Additionally, we showed that the expression of miR-146a-5p gradually increased in femurs with age not only in female mice but also in female patients, and miR-146a-5p deletion protected female mice from age-induced bone loss. These data suggested that miR-146a-5p has a crucial role in suppressing the bone formation and that inhibition of miR-146a-5p may be a strategy for ameliorating osteoporosis.

1. Introduction

miRNA is a kind of non-coding RNAs in the length of 20–24 nucleotide (nt). By affecting the stability and translation of RNAs, miRNAs play an important role in post-transcriptional regulation of gene expression in multicellular organisms (Ambros, 2004; Chitwood and Timmermans, 2010; Kosik, 2010; Rigoutsos and Furnari, 2010). Osteogenic differentiation and bone formation are complex processes and delicately regulated by numerous factors, among which are some miRNAs (Alliston and Derynck, 2002; Karsenty, 2003; Marx, 2004; Berger et al., 2019; Rendina-Ruedy and Rosen, 2020).

miR-146a, an important miRNA, is associated with divers diseases, including systemic lupus erythematosus (SLE), rheumatoid arthritis (RA), osteoarthritis (OA), osteosarcoma (OS), obesity, gastric cancer, and liver cancer, and similar conditions so on (Boldin et al., 2011; Hou et al., 2009; Iacona and Lutz, 2019; Karrich et al., 2013; Pauley et al., 2008; Qu et al., 2015; Tang et al., 2009; Zhang et al., 2017; Wu et al., 2016). Recent studies have started to focus on the relationship between miR-146a and bone-related diseases and have found that miR-146a has an important effect on bone formation and osteoblasts (Saferding et al., 2017; Ammari et al., 2018; Saferding et al., 2019; Zhao et al., 2019; Xie et al., 2017). However, certain target genes and the mechanisms by which miR-146a works on osteoblasts are not fully clear yet.

Recent evidence has suggested that Sirt1, a longevity gene, is also involved in regulating bone formation. Some studies have shown that Sirt1 knock-out (KO) not only contributed to the slowing of bone formation but also led to bone loss in mice (Xu et al., 2010; Gabay et al., 2012; Cohen-Kfir et al., 2011). Others found that Sirt1 inhibition suppressed the activity of growth plate chondrocyte, leading to the lack of longitudinal growth of metatarsal bone (Lemieux et al., 2005; Gabay et al., 2013).

In this study, we found that miR-146a-5p took part in the inhibition of osteoblast differentiation and was negatively correlated with bone formation. Further, we identified *Sirt1*, an enzyme deacetylating the

* Correspondence to: R. Lai, No 613 Huangpu Avenue, Tianhe District, Guangzhou 510630, China.
** Correspondence to: X. Wang, No. 37 Xueyuan Road, Haidian District, Beijing 100000, China.
E-mail addresses: prof.dr.lai@163.com (R. Lai), xiaogangwang@buaa.edu.cn (X. Wang).
[1] These authors contributed equally to this work.

https://doi.org/10.1016/j.bonr.2021.101013
Received 11 June 2020; Received in revised form 8 March 2021; Accepted 12 March 2021
Available online 15 March 2021

proteins responsible for cellular regulation, as a direct target of miR-146a-5p. We also found the age-relevant increase of miR-146a-5p in three subgroups of age, which indicated that miR-146a-5p was one of the factors causing bone loss in older female mice. Overall, our study provides new ideas for the future treatment of osteoporosis.

2. Materials and methods

2.1. Ethics statement

We complied with the human and animal experimental ethics including ARRIVE guidelines and the National Institutes of Health guide for the care and use of laboratory animals. The Committees of Clinical Ethics in The First Affiliated Hospital of Jinan University approved the clinical researches. Meanwhile, patients have been informed of the study procedures in detail before sampling. They observed their privacy rights and agreed to publish relevant personal information. The animal study was approved by the Ethics committee of the laboratory animal center at Jinan University.

2.2. Preparation of female patients' bone specimens

We estimated the sample size on the website (http://powerandsamplesize.com/). After excluding the patients who had diabetes, malignant tumor, or other serious diseases in the last 5 years, 45 bone specimens were randomly obtained from different bone-fractured individuals ranging from the age of 60 to 89 years. All of the participants were from The First Affiliated Hospital of Jinan University.

2.3. Female mice

Since the incidence of osteoporosis is much higher in females than in males, we chose female mice as the research object of this experiment. To choose the sample size of animals, we calculated the sample size on http://powerandsamplesize.com/ (the type-I error rate (alpha) is 0.05 and the power (1-beta) is 0.80), and we estimated sample size was 6. Wild-type (WT) and miR-146a KO female mice were purchased from Jackson laboratory, both of which were generated from the intercross of miR-146a+/− heterozygous female mice with a C57BL/6 background. All of the female mice were divided into experimental and control groups by using Permanent Random Numbers (PRNs), fed in a specific pathogen-free animal facility of laboratory animal center in Jinan University, and afterward sacrificed at the age of 2 or 12 months to gain the bone specimens.

2.4. Radiographic imaging

Firstly, we harvested the X-ray images of the entire femur from female mice by using a Faxitron X-ray system as recommended by the manufacturer (Wheeling). Next, the femurs were scanned *in vivo* at a voxel size of 10 μM with the help of μCT50 instruments (Scanco Medical, Switzerland). Besides, we reconstructed the trabecular structure beneath the most distal aspect of the growth plate. Eventually, the following parameters: the ratio of bone volume to tissue volume (BV/TV), bone mineral density (BMD), trabecular bone number (Tb. N), trabecular bone thickness (Tb. Th), trabecular bone separation (Tb. Sp), bone formation rate (BFR/BS) and mineral apposition rate (MAR) were analyzed at a setting of Sigma = 1. 2, supports = 2 and threshold = 180.

2.5. Haematoxylin and eosin (H&E) staining

Firstly, we fixed the femurs from the WT and miR-146a KO female mice with a 4% paraformaldehyde (PFA) solution. After that, we decalcified the bone tissues in 10% EDTA for 21 days, embedded them into paraffin, and sliced them at a thickness of 4 nm. Lastly, we performed the H&E staining following the manufacturer's protocol.

2.6. Alizarin red staining

BMSCs isolated from 2-month-old WT and miR-146a KO female mice were cultured in the osteogenic Alpha Modified Eagle's Medium (α-MEM) (Invitrogen) containing 10% FBS, 1% penicillin-streptomycin, 5 mM β-glycerol phosphate (Sigma), 0.1 mg/ml ascorbic acid (Sigma) and 10 nM dexamethasone (Sigma) and the mediums were replaced every 2–3 days. After 21 days, the cells were washed three times with PBS and fixed in 4% PFA for 15 min. Then, 40 mM Alizarin red S (pH = 4. 0, Sigma) was used to stain the cells for 15 min.

2.7. Double-labeling analysis

Firstly, both WT and miR-146a KO female mice were injected with xylenol orange (10 mg/kg) and after 2 weeks calcein green (20 mg/kg) *via* intraperitoneal injection. 12 h after the last injection, all-female mice were sacrificed to gain the femurs. Then, we fixed the femurs with a 4% PFA solution for 24 h subsequently embedded them in light-cured resin (EXAKT 7200 VLC) for 13. 5 h. After that, we sliced them at a thickness between 15 and 20 μm and mounted the section with 4, 6-diamidino-2-phenylindole (DAPI, Sigma). Finally, a confocal microscope (Leica image analysis system, Q500MC) was used to capture the images.

2.8. Immunohistochemistry

To detect dentin matrix protein 1 (DMP1) in the matrix of femurs from WT and miR-146a KO female mice, we fixed them with 4% PFA and embedded them in paraffin. After slicing, we incubated the tissue sections with anti-DMP1 antibody (monoclonal, clone 8G10.3) diluted 1:300 in goat serum at 4 °C and after 24 h rabbit anti-mouse secondary antibody (MXB, KIT-9706). Finally, a light microscope was used to observe the sections.

2.9. Cell culture

The mouse preosteoblast MC3T3-E1 clone 4 cell line (authenticated by immunofluorescence staining, not contaminated by mycoplasmas) was kept in α-MEM (Invitrogen) providing 10% FBS (Gibco) and 1% penicillin together with streptomycin (Invitrogen). Besides, the cells were cultured in 5% CO_2 and 95% humidity and discarded when over the 10th passage. For the experiments, confluent cells were isolated with 0.25% trypsin containing 10 mM EDTA.

2.10. Cell transfection and cell lysis

MC-3T3 E1 cells were transfected with miRNAs at a final concentration of 100 nM using Lipofectamine RNAi MAX (Invitrogen) according to the manufacturer's protocol. The microRNA mimics were synthesized by Shanghai Integrated Biotech Solutions Co., Ltd. The seed sequences of the miR-146a-5p were mutated and the detailed sequences of the miR-146a-5p mimics and its mutants were given in Supplementary Table 1. In miRNA pulldown assay, corresponding biotinylated miRNAs were used. As for AGO2 immunoprecipitation, miR-NC and miR-146a-5p were transfected. 24 h post-transfection, the medium was changed. 48 h after cell transfection, cells were collected and lysed using 550 μl lysate buffer (20 mM Tris, pH = 7. 5, 200 mM NaCl, 2. 5 mM $MgCl_2$, and 0.5% NP-40) in the presence of protease inhibitor and RNase inhibitor.

2.11. Sirt1 3′UTR cloning and dual-luciferase assay

The corresponding sequencing of *Sirt1* mRNA 3′UTR in the *Sirt1* gene (gene ID 93759) was amplified by PCR and then constructed into the *Xho*I site downstream of the stop codon in the pGL3-CMV-LUC-MCS firefly luciferase vector (Promega). The sequences of the 3′ UTR region of Sirt1 and the clone primers were provided in the Supplementary

document. For the luciferase assay, MC3T3-E1 cells were plated onto six-well plates at a density of 1 × 10^6 cells per well. After transfecting miRNAs described above, 200 ng *Sirt1*-pGL3 recombinant and the internal control of 50 ng pRL-TK *Renilla* luciferase plasmid (Promega) were co-transfected into the cells as suggested by the manufacturer. The value of fluorescence detected by the luminometer (Glomax, Promega) was used to quantify the luciferase activity.

2.12. RNA pulldown assay

We first had the miRNAs synthesized by using Transcript Aid T7 high-yield transcription kit (Thermo Fisher). Subsequently, the biotinylated miRNAs were purified with a Biotin RNA Labelling Mix (Thermo Fisher) and miRNeasy Mini Kit (QIAGEN) respectively. Before transfection, MC3T3-E1 cells were replanted at a suitable density in a 10 cm tissue culture dish to ensure they were ≤80% confluent until collecting. After cell transfection and cell lysis as explained above, cell lysates were centrifuged at 18000 r.p.m. For 10 min at 4 °C and supernatant was harvested. To pulldown the biotin-miRNA-mRNA complex, every 500 μl supernatant was mixed with 50 μl streptavidin agarose beads (Thermo Fisher) and incubated overnight on the rotating wheel. Finally, RNAs from the biotin-labeled sample and input sample were extracted as hereunder mentioned for real-time PCR analysis.

2.13. RNA immunoprecipitation

After cell transfection and cell lysis described above, we centrifuged the MC3T3-E1 cell lysates at 12,000 r.p.m. For 15 min at 4 °C and collected the supernatant. Next, the supernatant was incubated with RIP buffer (150 mM KCl, 25 mM Tris, pH = 7.4, 5 mM EDTA 0.5 mM dithiothreitol, and 0.5% NP-40) supplemented with mouse anti-AGO2 antibody (Abcam, Cambridge, MA, USA) or negative control mouse IgG (Millipore) on a rotator overnight at 4 °C. To obtain the antibody-AGO2-miRNA-mRNA complex, 40 μl of protein A/G plus-agarose beads (Santa Cruz Biotechnology, Santa Cruz, CA) were mixed into the supernatant and incubated with gentle rotating at 4 °C. 1 h later, centrifugation was performed at 2500 r.p.m. For minutes and supernatant was gained. Eventually, RNAs were isolated for real-time PCR analysis as described below.

2.14. RNA extraction and real-time PCR analysis

We firstly homogenized the bone specimens with a high-speed agitation, Polytron blender (Kinematica, Luzern, Switzerland). To extract total RNA, RNAiso Plus reagent (Takara) was used for BMSCs lysates, MC3T3-E1 cell lysates, and bone specimens. Next, RNA RT reactions were conducted with a PrimeScript RT reagent Kit and a genomic DNA Eraser (Perfect Real Time) (Takara) following the manufacturer's instruction. In the end, quantitative real-time PCR was accomplished by using an SYBR Premix Ex Taq II kit (Takara). Primer sequences used for qPCR were provided in Supplementary Table 2. Small nuclear RNA *U6* was selected as an internal reference of miR-146a-5p and the housekeeping gene *Actin* was selected as an internal reference of mRNA.

2.15. Detection of type I collagen (collagen I) in the supernatant

Suggested by the manufacturer, we firstly pipetted 75 μl supernatant containing collagen I protein or the corresponding controls into ELISA plates in the type I collagen assay kit (Metra Biosystems, CA, USA), which were pre-coated with the antibody. Then, 25 μl mouse IgG antibody solution was added to the wells of the plate and incubated for 60 min on a shaking table at room temperature. Eventually, washing buffer (25 mM Tris and 50 nm NaCl, pH = 7.2) was used to wash the plates three times at room temperature.

2.16. Western blot analysis

MC-3T3 E1 cells were lysed in lysis buffer (50 mM Tris, pH = 7. 5, 250 mM NaCl, 0.1% SDS, 2 mM dithiothreitol (DTT), 0.5% NP-40) supplemented with 1 mM PMSF and protease inhibitor cocktail for 30 min on ice. Protein fraction was collected by centrifugation at 15,000*g* at 4 °C for 10 min and its concentration was quantified by the bicinchoninic acid method. Next, protein extract was subjected to SDS–PAGE and transferred onto polyvinylidene difluoride membranes by electroblotting at 300 mA for 85 min. The membranes were blocked with 5% BSA and incubated with specific antibodies overnight at 4 °C with gentle rotating. HRP-conjugated secondary antibodies were added, incubated for 1 h with shaking, and visualized using an enhanced chemiluminescence kit (Pierce). The antibodies, which we used to examine the concentrations of Sirt1 and GAPDH in the lysates respectively, included mouse Sirt1 (Santa Cruz, sc-74465, 1:100) and mouse GAPDH (Santa Cruz, sc-365062, 1:100). And the conjugated secondary antibody was anti-rabbit IgG (1:5000, E030120, EarthOx).

2.17. Statistics and reproducibility

All data are presented as the mean ± s.e.m. Significant differences between the two groups were determined by unpaired Student's *t*-test (two-tailed). Significant differences between multiple groups were determined by one-way ANOVA with Dunnett's multiple comparisons test. A *P*-value of less than 0.05 was considered statistically significant. n.s., not significant, $*P < 0.05$, $**P < 0.01$, $***P < 0.005$. GraphPad Prism version 8.0 was used for all statistical analyses. The experiments of histomorphological staining, immunohistochemical staining, and western blot analysis were repeated three times independently with similar results.

3. Results

3.1. miR-146a-5p KO female mice have increased trabecular bone

To investigate the role of miR-146a-5p in regulating bone mass *in vivo*, we established a miR-146a KO mouse model and radiographed the whole femur from 2-month-old wild-type (WT) and miR-146a KO female mice by micro-computed tomography (micro-CT). Reconstruction of the trabecular bone showed that WT displayed lower bone mass than miR-146a KO female mice (Fig. 1a). Consistently, the result of H&E staining presented reduced density of the trabecular bone in the femurs from WT when compared with the miR-146a KO female mice (Fig. 1b). Analysis of the bone mass parameters showed a lower level of BV/TV, BMD, Tb. N, and Tb. Th, but a higher level of Tb.Sp in the femurs from WT but not in those from miR-146a KO female mice (Fig. 1c–g). These findings are consistent with recent reports that miR-146a contributed to a lower level of bone mass in mice (Saferding et al., 2019).

3.2. miR-146a-deficient female mice show the enhanced bone formation

To assess the function of miR-146a-5p in bone formation *in vivo*, we analyzed the dynamic histomorphometric changes of femurs in the WT and miR-146a KO female mice after birth. Compared with miR-146a KO female mice, the double-labeling analysis showed the shorter distance between xylenol orange and calcein green, lower BFR/BS, and lower MAR of femurs from WT, which suggested that the presence of miR-146a-5p slowed down the process of bone formation (Fig. 2a, b). Anti-DMP1 immunohistochemical staining also showed that the bone mineralization of femurs from WT was weaker than miR-146a KO female mice (Fig. 2c). Consistent with the changes in staining, fewer *Bglap* (osteocalcin) and *Alp* (alkaline phosphatase) mRNA were detected in WT than in miR-146a KO female mice by real-time PCR (Fig. 2d). All these data indicated that miR-146a was responsible for the slow bone formation in mice.

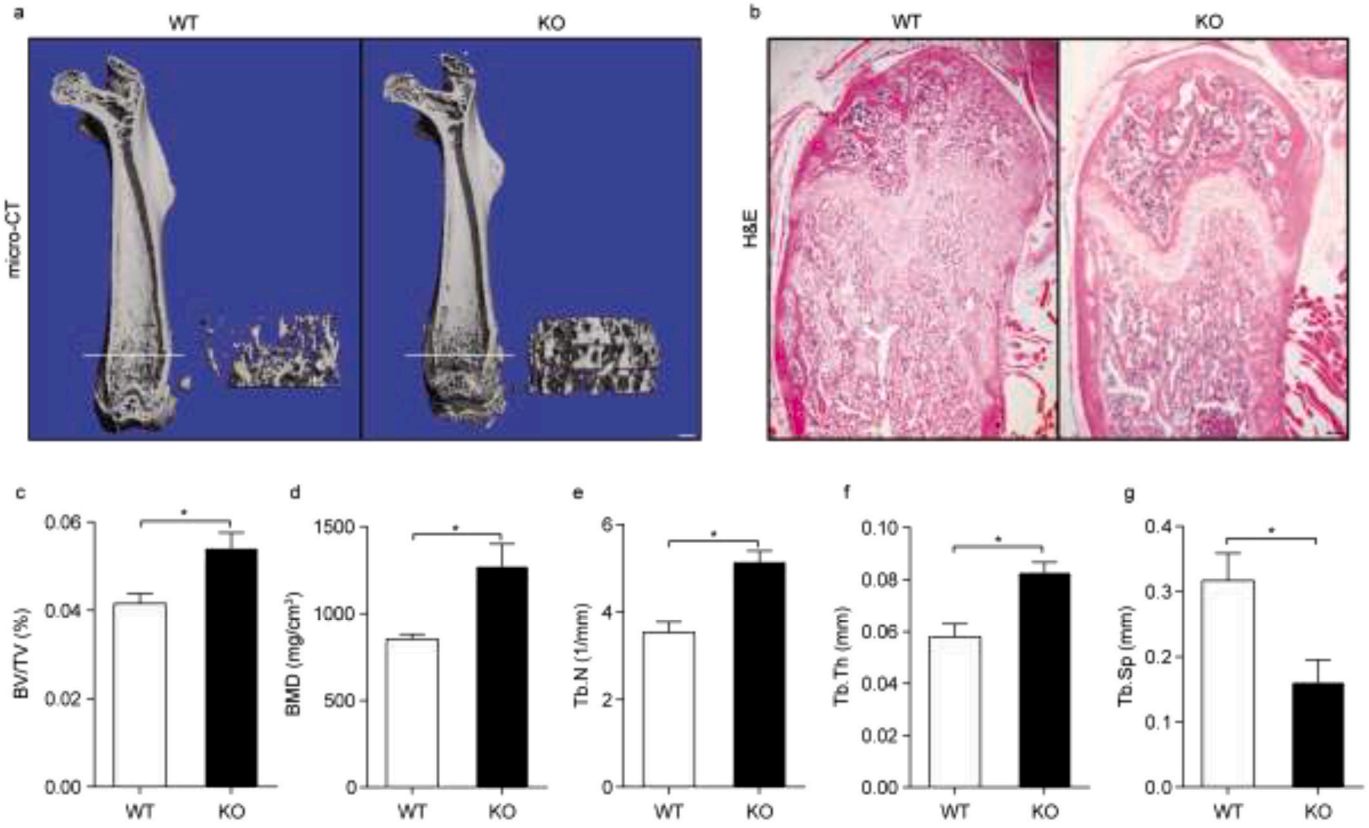

Fig. 1. miR-146a-5p KO female mice have increased trabecular bone. (a) Representative micro-CT images showing the architectures of the trabecular bone of femurs from 2-month-old WT and miR-146a KO female mice in three dimensions (bars = 1 mm). (b) H&E staining images of femurs from 2-month-old WT and miR-146a KO female mice (bars = 200 μm). Relevant analysis of bone mass parameters for (c) BV/TV, (d) BMD, (e) Tb.N, (f) Tb.Th and (g) Tb.Sp of femurs from 2-month-old WT and miR-146a KO female mice ($n = 6$). Data are presented as the mean ± s.e.m. Significant differences between the two groups were determined by unpaired Student's *t*-test (two-tailed), $^*P < 0.05$.

3.3. Osteoblast differentiation takes place faster in miR-146a-deficient BMSCs

After observing the close connection between miR-146a-5p and bone tissue, we next decided to explore what miR-146a-5p would do to BMSCs *in vitro*. First, we cultured the BMSCs derived from femurs in an osteogenic medium. After 21 days, we assessed calcium deposition using Alizarin red staining and found that in the medium of WT BMSCs, the color remained light, while in the medium of miR-146a KO female mice BMSCs, the color became deep (Fig. 3a). Optical density (*OD*) was quantified at 562 nm wavelength by a multi scanner Autotrader (Biotech Instruments, NY, US) and showed statistically significant differences in calcium deposition between WT and miR-146a KO female mice (Fig. 3b). Thus, we speculated that miR-146a-5p might restrain osteoblast differentiation of BMSCs. To verify this, we collected collagen I protein in the supernatant to assess collagen levels and found that the production of collagen I protein was also lesser in WT compared with miR-146a KO female mice BMSCs (Fig. 3c). Similarly, weakened expression of *Bglap* and *Alp* mRNA was found in WT female mice BMSCs by real-time PCR (Fig. 3d). These discoveries collectively provide evidence that miR-146a functionally hinders the osteoblast differentiation program of BMSCs *in vitro*.

3.4. miR-146a-5p directly targets Sirt1 in osteoblasts

To obtain more information about the principle by which miR-146a-5p acts on BMSCs, we used Miranda to predict mRNAs targeted by miR-146a-5p. Among the candidate targets, we noticed that *Sirt1* mRNA had a miR-146a-5p binding site in its 3′ untranslated region (UTR). Using TargetScan, we discovered that miR-146a-5p binding sites in *Sirt1* mRNA were identical in numerous species including humans (Fig. 4a). To determine whether miR-146a-5p directly targets *Sirt1*, we performed dual-luciferase reporter assay in MC3T3-E1 cells by using luciferase reporters constructed with *Sirt1* 3′UTR containing the miR-146a-5p binding site, in which the seed sequence of the reporter was not mutated. We found that luciferase reporter activity of the *Sirt1* 3′UTR was significantly suppressed by miR-146a-5p compared with the miR-146a-5p negative control (miR-NC) and the two sequences altered version of miR-146a-5p (miR-MUT) (Fig. 4b). To further validate the interaction between miR-146a-5p and *Sirt1* mRNA, we conducted biotin-miR-146a-5p pulldown analysis and AGO2 RNA immunopurification (RIP) assays in MC3T3-E1 cells. AGO2 is the core component of RNA-induced silencing complex (RISC), whose assembly is a precondition for the binding between miRNA and its target mRNA resulting in small RNA-mediated gene silencing (Yoda et al., 2010). As expected, biotin-miR-146a-5p is combined with much more *Sirt1* mRNA than the biotin-miR-NC and biotin-miR-146a-5p mutants in MC3T3-E1 cells (Fig. 4c). Consistently, the results of AGO2 RIP assays demonstrated that miR-146a-5p was incorporated into RISC containing AGO2 and subsequently targeted *Sirt1* specifically but miR-NC did not (Fig. 4d). We quantified SIRT1 protein by Western blot to explore the suppressive effect of miR-146a-5p on *Sirt1* mRNA translation (Fig. 4e). ImageJ analysis showed that SIRT1 protein in MC3T3-E1 cells was functionally down-regulated after the miR-146a-5p treatment, establishing that miR-146a-5p took part in the post-transcriptional expression inhibition of *Sirt1* (Fig. 4f). To strengthen the hypothesis about *Sirt1* being a key mediator of the observed phenotype, a Western-blot assay was conducted to evaluate the protein expression levels of *Sirt1* in both WT and

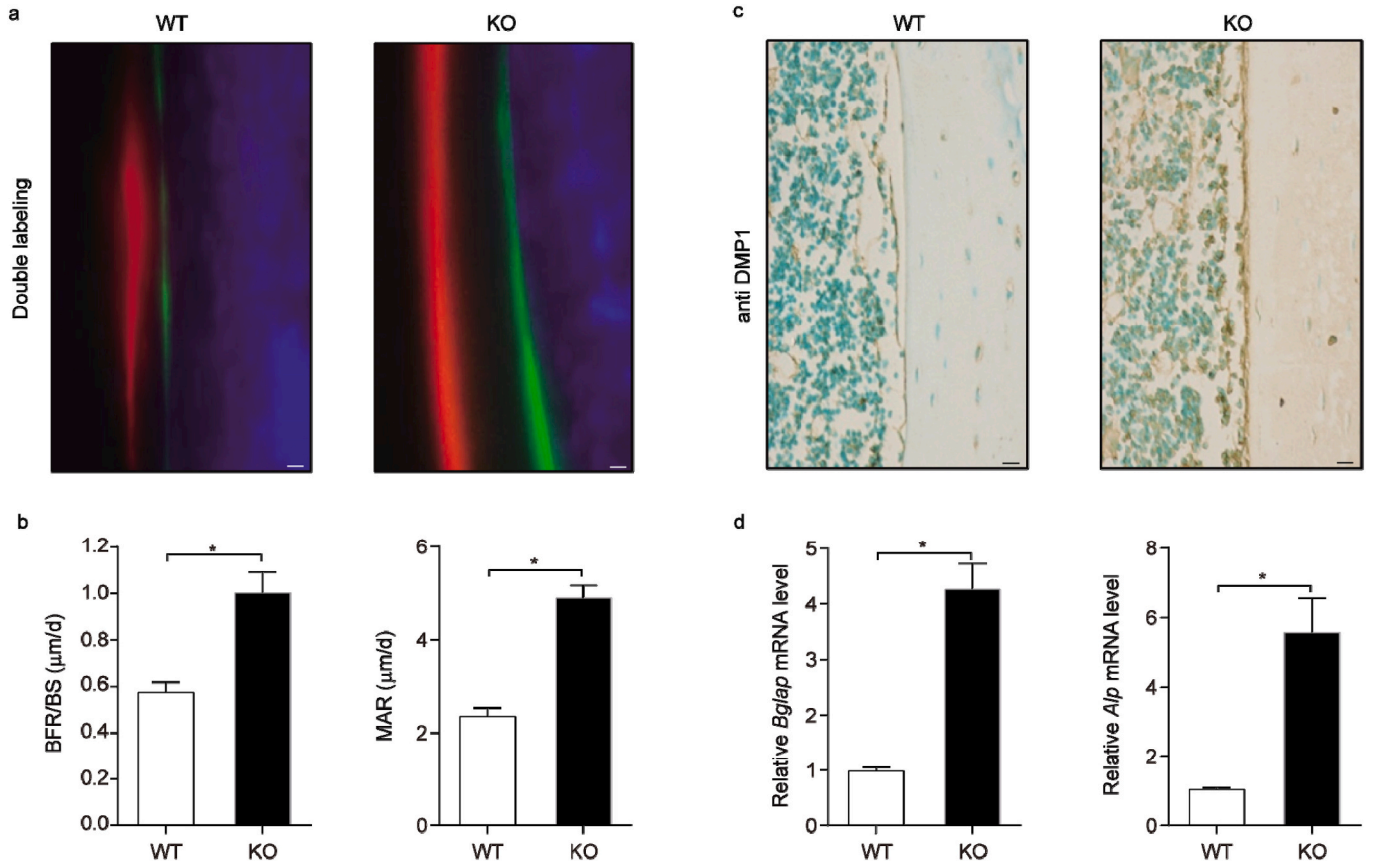

Fig. 2. miR-146a-deficient female mice show enhanced bone formation. (a) Representative images of xylenol orange and calcein green labeling in femurs of 2-month-old WT and miR-146a KO female mice (bars = 40 μm) and (b) statistical analysis of bone formation parameters of BFR/BS as well as MAR (n = 6). (c) Anti-DMP1 immunohistochemical staining images of femurs from 2-month-old WT and miR-146a KO female mice (bars = 40 μm). (d) Real-time PCR analysis of *Bglap* and *Alp* mRNA levels in femurs from 2-month-old WT and miR-146a KO female mice (n = 6). Data are presented as the mean ± s.e.m. Significant differences between the two groups were determined by unpaired Student's t-test (two-tailed), $^*P < 0.05$.

KO mice (Fig. 4g). The results showed that there was a significant up-regulation of the *Sirt1* expression levels in miR-146a KO mice (Fig. 4h). Collectively, these data provide strong evidence that miR-146a regulates bone mass by targeting *Sirt1* mRNA in osteoblasts.

3.5. *miR-146a-deficient female mice are resistant to aging-induced bone loss*

To investigate whether genetic suppression for miR-146a-5p could rescue bone loss induced by aging, we captured radiographs of the entire femoral bone by X-ray and micro-CT from euthanized 12-month-old WT and miR-146a KO female mice and then analyzed the microarchitecture parameters quantitatively to assess the statistical significance of any difference in their femurs. X-ray analysis showed miR-146a KO female mice to have marginally thicker femoral shafts and more obvious high-density images in the marrow cavity region than WT (Fig. 5a). Similarly, the three-dimensional images of the trabecular structure after reconstruction from femurs by micro-CT showed larger amounts of trabecular bone and bone of greater diameter in miR-146a KO female mice than WT (Fig. 5b). Moreover, analysis of BV/TV, Tb. N, and Tb. Th indicated that these three bone mass parameters increased consistently in miR-146a KO female mice, and this was closely consistent with the changes shown in other images (Fig. 5c–e). These results collectively suggest that miR-146a deletion can reverse aging-induced bone loss and may protect mice from osteoporosis.

3.6. *miR-146a-5p expression increases in bone specimens of older female mice and female patients*

Fabiola Olivieri et al. have shown that miR-146a was a marker of senescence-associated pro-inflammatory status in cells involved in vascular remodeling (Olivieri et al., 2013). To evaluate the mechanisms that may underlie how miR-146a-5p regulates aging-induced bone loss under physiological conditions, we evaluated the expression of miR-146a-5p in bone specimens from 2- and 12-month-old WT female mice. We found more miR-146a-5p was produced in older female mice (Fig. 6a). On this basis, we collected bone specimens from humans in three subgroups stratified by age. Real-time PCR analysis showed that the level of miR-146a-5p was visibly higher in older humans, and it shared analogous age-associated changes in miR-146a-5p expression with female mice (Fig. 6b). These findings in which the expression of miR-146a was positively correlated with age indicate that high levels of miR-146a expression in the elderly may explain the cause of osteoporosis.

4. Discussion

In this study, we used the miR-146a KO mouse model to establish the role of miR-146a-5p in regulating bone mass *in vivo* and performed biotin-miRNA pulldown assay and AGO2 IP analysis to identify its target mRNA *in vitro*. In young mice, osteoblast differentiation in miR-146a KO female mice takes place faster than in WT. This is the reason why miR-146a KO female mice have higher bone mass and faster bone formation than WT. Further investigations showed that miR-146a-5p directly

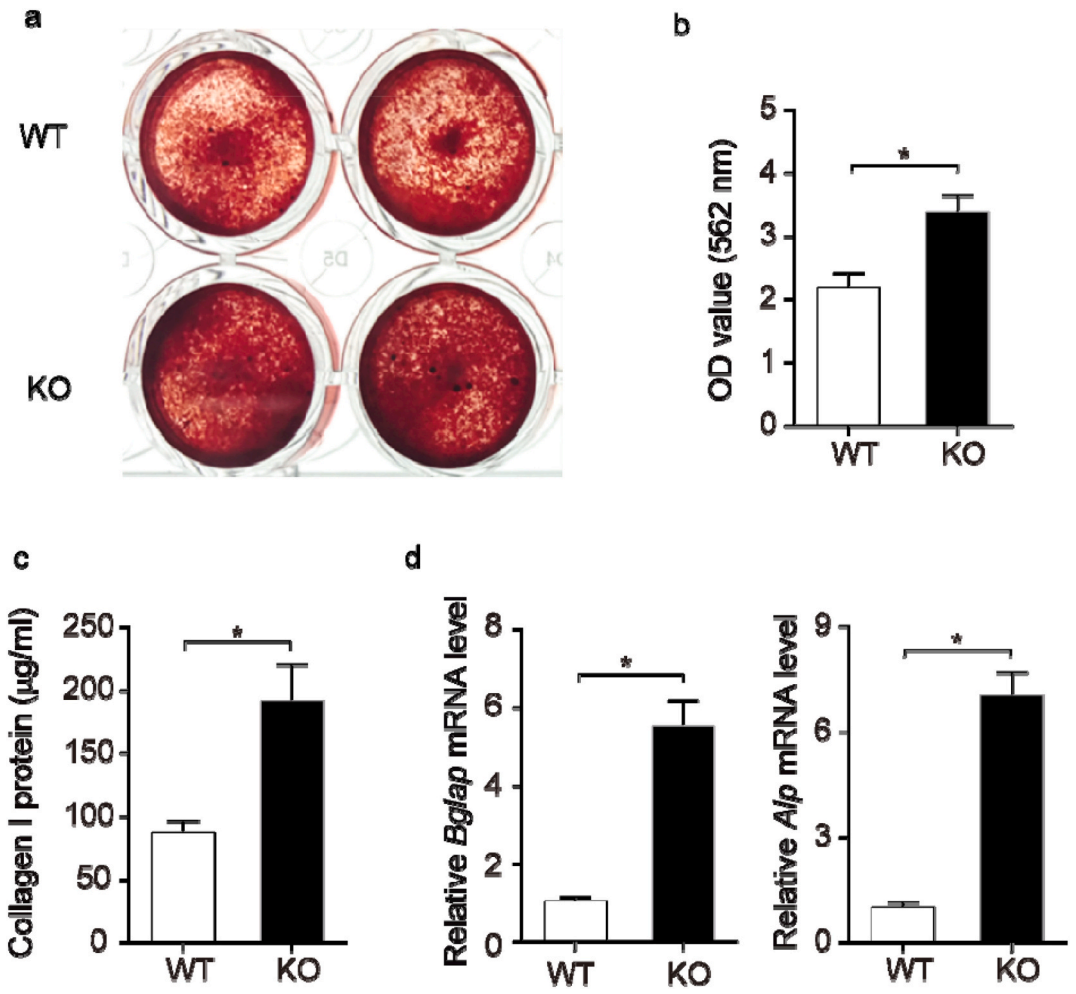

Fig. 3. Osteoblast differentiation takes place faster in miR-146a deficient BMSCs. (a) Alizarin red staining of the mineralized matrix from 2-month-old WT and miR-146a KO female mice BMSCs after 21 days' osteogenesis induction. The BMSCs numbers of WT and miR-146a KO female mice are almost identical. (b) Quantification analysis of alizarin red staining for 2-month-old WT and miR-146a KO female mice ($n = 6$) BMSCs appeared as *OD* value at 562 nm wavelength. (c) Assessment of collagen I protein levels in the supernatant of BMSCs from 2-month-old WT and miR-146a KO female mice ($n = 6$). (d) Real-time PCR analysis of *Bglap* and *Alp* mRNA in BMSCs from 2-month-old WT and miR-146a KO female mice ($n = 6$). Data are presented as the mean ± s.e.m. Significant differences between the two groups were determined by unpaired Student's *t*-test (two-tailed), $^*P < 0.05$.

targets *Sirt1* mRNA in osteoblasts. The phenomena of less bone loss in aged miR-146a KO female mice than WT and increased miR-146a-5p expression in older individuals among both female mice and female patients indicate that suppression of miR-146a-5p may be a feasible therapeutic means of preventing aging-induced bone loss.

First, we noticed that bone mass was greater in miR-146a KO female mice, which is consistent with the findings of a recent report that there was a more trabecular bone mass in miR-146a KO mice than in WT mice starting at the age of 6 months (Saferding et al., 2019). miR-146a is of great importance to and plays a complicated role in bone metabolism. Xie Q et al. showed miR-146a was a negative regulator in osteogenesis and bone regeneration from adipose-derived mesenchymal stem cells (ADSCs) both *in vitro* and *in vivo* (Xie et al., 2017). In contrast, Cheung KS et al. suggested that miR-146a negatively regulated chondrogenesis and might indirectly promote osteogenic differentiation of human fetal femur-derived skeletal stem cells (Cheung et al., 2014). Previous works have shown that the expression of mir-146a can inhibit osteoclastogenesis (Nakasa et al., 2011). In our study, we found that the bone mass of miR-146a KO female mice was higher than WT due to enhanced bone formation. This is closely consistent with the aberrant myeloproliferation and histologically and immunophenotypically defined myeloid sarcomas in miR-146a deletion mice (Boldin et al., 2011; Magilnick et al., 2017; Zhao et al., 2011).

We then explored how miR-146a-5p acted on MC-3T3 E1 cells. Zhao J et al. found that miR-146a can inhibit OB differentiation, but no studies have been performed on its target gene in osteoblasts (Zhao et al., 2019). In our study, miR-146a-5p regulated osteoblasts at the post-transcriptional level by binding *Sirt1* mRNA. Sirtuin1 (Sirt1) is an NAD+-dependent deacetylase that plays a significant role in aging. Osteoporosis is one of the common features of aging (Herranz et al., 2010). It has been reported that *Sirt1* can inhibit NF-κB-induced osteoclast differentiation and increase bone mass in ovariectomized female mice by down-regulating sclerostin (Artsi et al., 2014; Edwards et al., 2013). The deletion of *Sirt1* in osteoblasts would increase bone absorption. Thus, *Sirt1* activation by activator is here considered a suitable therapy for osteoporosis.

Next, we investigated the influence of miR-146a deletion in bone loss induced by aging. Osteoporosis and osteoporotic fractures are worldwide public health challenges, and one of the main causes is aging (Li et al., 2017). We found less bone loss in older miR-146a KO female mice than in similarly aged WT. We believe the inhibition of *Sirt1* translation by miR-146a-5p was weakened in older miR-146a KO female mice, such that more SIRT1 proteins were produced to suppress osteoclast differentiation and increase bone mass as described in the paragraph above.

Eventually, we probed the miR-146a-5p expression to evaluate how it changed with age. By detecting the levels of miR-146a-5p expression

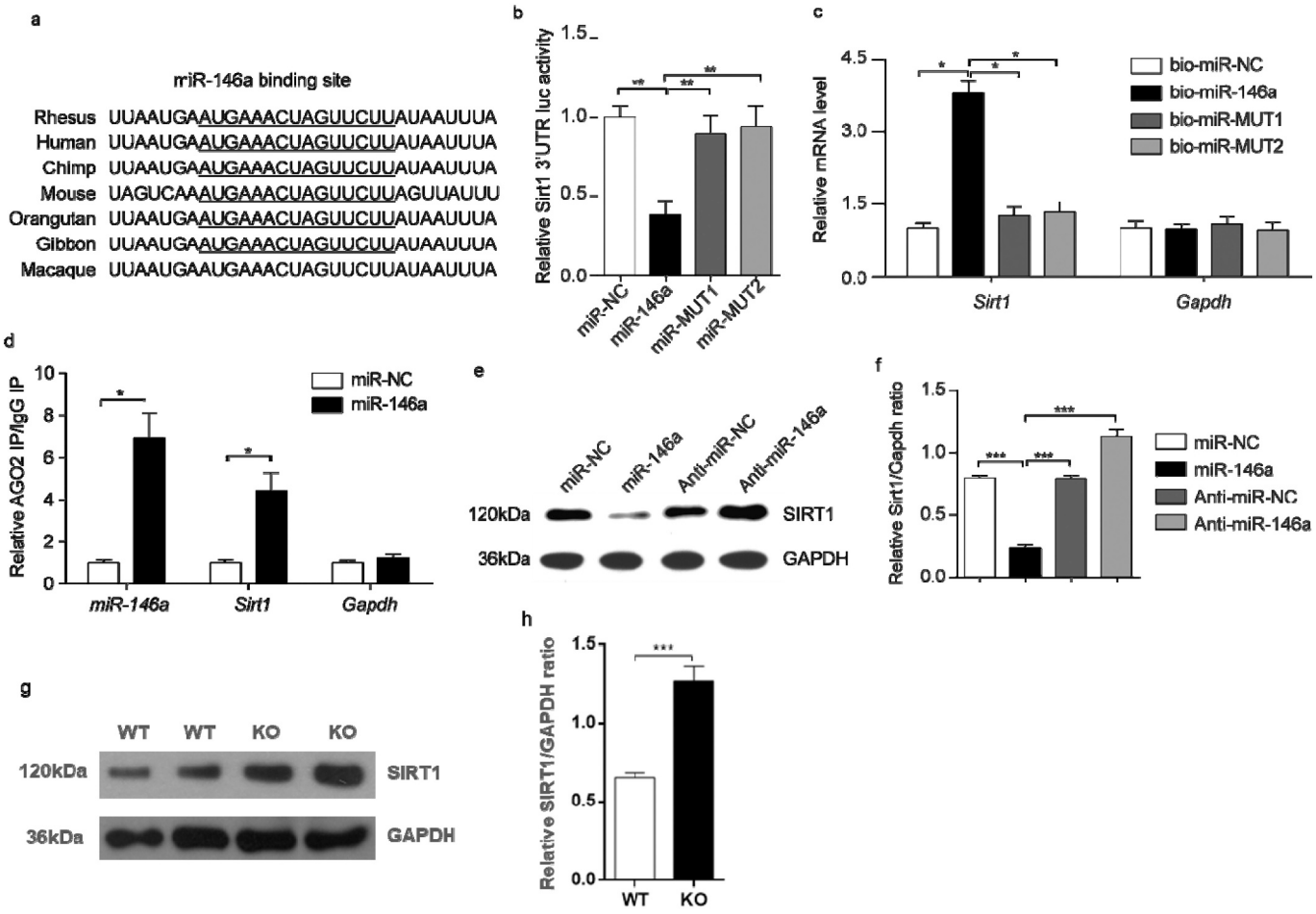

Fig. 4. miR-146a-5p directly targets *Sirt1* in osteoblasts. (a) The conserved binding sites of miR-146a-5p across species. (b) Luciferase activity assay of *Sirt1* 3′ UTR reporter in MC3T3-E1 cells administered with miR-146a-5p, miR-146a-5p negative control (miR-NC), or the two sequences altered version of miR-146a-5p (miR-MUT) ($n = 6$). The seed sequence of the reporter was not mutated. (c) Biotin-miRNA pulldown of *Sirt1* mRNA in MC3T3-E1 cells transfected with bio-miR-NC, bio-miR-146a-5p, and bio-miR-146a-5p mutations, respectively (n = 6). (d) AGO2 IP analysis of the interaction between miR-146a-5p and *Sirt1* mRNA. The levels of miR-146a, *Sirt1* mRNA, and *Gapdh* mRNA were quantified by real-time PCR and the amounts of precipitated AGO2 protein were normalized to the control IgG protein ($n = 6$). (e) Western blot analysis of SIRT1 protein levels in MC3T3-E1 cells transfected with miR-NC, miR-146a-5p, anti-miR-NC, or anti-miR-146a-5p after 48 h. (f) Quantification analysis of SIRT1 protein levels in MC3T3-E1 cells transfected with miR-NC, miR-146a-5p, anti-miR-NC, or anti-miR-146a-5p after 48 h was performed on ImageJ software (n = 6). (g) Western blot analysis of SIRT1 protein levels in both WT and KO mice. (h) Quantification analysis of SIRT1 protein levels in both WT and KO mice was performed on ImageJ software (n = 6). Data are presented as the mean ± s.e.m. Significant differences between the two groups were determined by unpaired Student's *t*-test (two-tailed). Significant differences between multiple groups were determined by one-way ANOVA with Dunnett's multiple comparisons test. $^{*}P < 0.05$, $^{**}P < 0.01$, $^{***}P < 0.005$.

in both female mice and female patients, we ascertained that female mice and female patients share similar age-relevant miR-146a-5p expression patterns, which suggested that miR-146a-5p in female patients seem to play the same role as it does in female mice. miR-146a-5p may also target *SIRT1* mRNAs in humans and suppress their expression, resulting in the phenomenon of bone loss in aged people, though the present study does not confirm this.

Further works should investigate the target gene and verify the function of miR-146a-5p in humans to confirm the transformation of miR-146a-5p in clinical settings based on our study. It is also valuable to perform more efforts such as target inhibition systems towards miR-146a-5p in osteoblasts to validate whether miR-146a-5p is a suitable therapeutic target for aging-related bone loss. What's more, whether the performance of miR-146a in male mice is similar to those in female mice still needs to be explored, for this experiment only focuses on the female. Even so, our research established that miR-146a-5p targeted *Sirt1* to regulate aging-induced bone loss induced *in vitro* and *in vivo*.

Transparency document

The Transparency document associated with this article can be found, in the online version.

CRediT authorship contribution statement

Mingxia Zheng: Data curation, Formal analysis, Investigation, Methodology, Validation, Visualization, Writing - original draft. **Junlong Tan:** Data curation, Formal analysis, Investigation, Methodology, Validation, Visualization, Writing - original draft. **Xiangning Liu:** Data curation, Formal analysis, Investigation, Methodology, Validation, Visualization, Writing - original draft. **Fujun Jin:** Formal analysis, Methodology, Validation, Visualization, editing - revised manuscript. **Renfa Lai:** Conceptualization, Project administration, Supervision, Writing - review & editing. **Xiaogang Wang:** Conceptualization, Project administration, Supervision, Writing - review & editing.

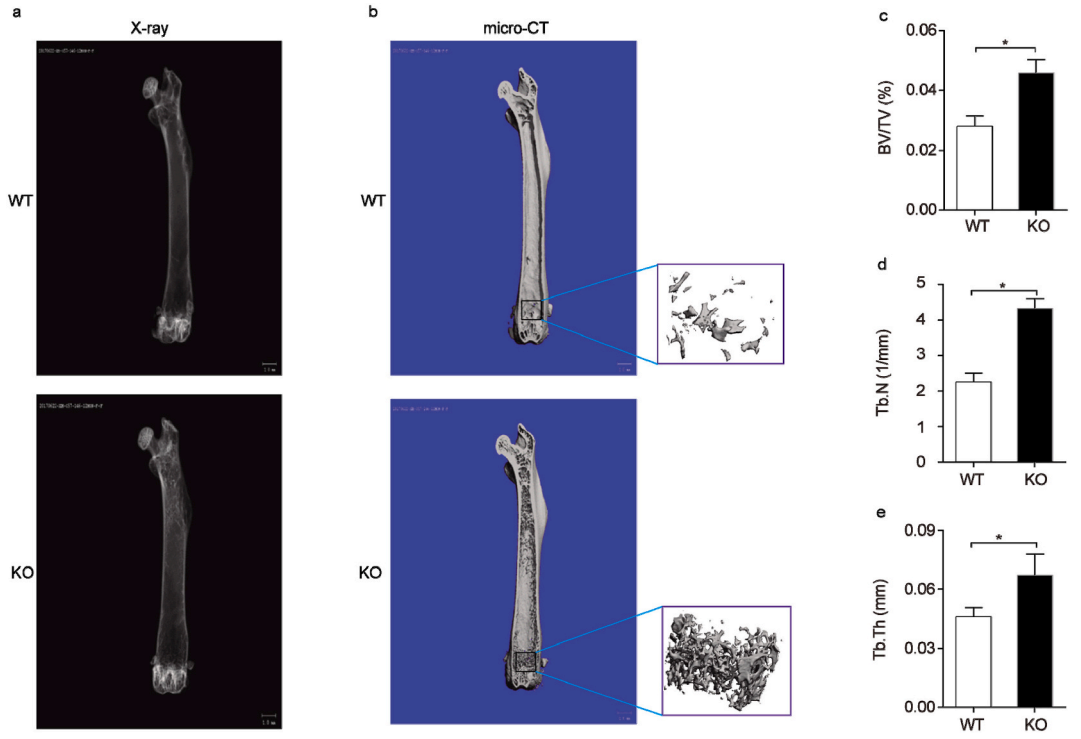

Fig. 5. miR-146a deficient female mice resist aging-induced bone loss. (a) Representative X-ray images (bars = 1 mm) and (b) micro-CT images showing the whole femur and the trabecular bone in three-dimension from 12-month-old WT and miR-146a KO female mice. A relevant analysis of bone mass parameters for (c) BV/TV, (d)Tb. N and (e) Tb.Th of femurs from 12-month-old WT and miR-146a KO female mice ($n = 6$). Data are presented as the mean ± s.e.m. Significant differences between the two groups were determined by unpaired Student's *t*-test (two-tailed), $^*P < 0.05$.

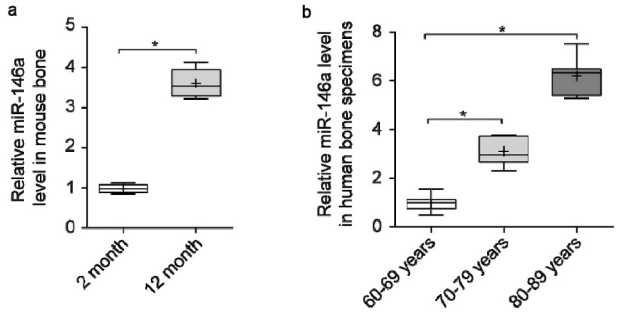

Fig. 6. miR-146a-5p expression increases in bone specimens of older female mice and female patients. (a) Real-time PCR analysis of miR-146a-5p in bone specimens from 2- and 12-month-old WT female mice ($n = 6$). The levels were related to the mean value of the 2-month group. (b) Real-time PCR analysis of miR-146a-5p in bone specimens from three subgroups of aged individuals ($n = 15$). The levels were normalized by the mean value of 60–69 group. Data are presented as the mean ± s.e.m. Significant differences between the two groups were determined by unpaired Student's *t*-test (two-tailed). Significant differences between multiple groups were determined by one-way ANOVA with Dunnett's multiple comparisons test. $^*P < 0.05$.

Declaration of competing interest

None.

Acknowledgments

This work was supported by grants from the National Natural Science Foundation of China (No. 81770873 and 81802193) and the Natural Science Foundation of Guangdong Province (2018A030313604). The funding source doesn't involve in the study design, the collection, analysis, and interpretation of data, writing of the report, or the decision to submit the article for publication.

Appendix A. Supplementary data

Supplementary data to this article can be found online at https://doi.org/10.1016/j.bonr.2021.101013.

References

Alliston, T., Derynck, R., 2002. Interfering with bone remodelling. Nature 416, 686–687.
Ambros, V., 2004. The functions of animal microRNAs. Nature 431, 350–355.
Ammari, M., Presumey, J., Ponsolles, C., Roussignol, G., Roubert, C., Escriou, V., Toupet, K., Mausset-Bonnefont, A.-L., Cren, M., Robin, M., 2018. Delivery of miR-146a to Ly6Chigh monocytes inhibits pathogenic bone erosion in inflammatory arthritis. Theranostics 8, 5972.
Artsi, H., Cohen-Kfir, E., Gurt, I., Shahar, R., Bajayo, A., Kalish, N., Bellido, T.M., Gabet, Y., Dresner-Pollak, R., 2014. The Sirtuin1 activator SRT3025 down-regulates sclerostin and rescues ovariectomy-induced bone loss and biomechanical deterioration in female mice. Endocrinology 155, 3508–3515.
Berger, J.M., Singh, P., Khrimian, L., Morgan, D.A., Chowdhury, S., Arteaga-Solis, E., Horvath, T.L., Domingos, A.I., Marsland, A.L., Yadav, V.K., Rahmouni, K., Gao, X.B., Karsenty, G., 2019. Mediation of the acute stress response by the skeleton. Cell Metab 30, 890–902.e8.
Boldin, M.P., Taganov, K.D., Rao, D.S., Yang, L., Zhao, J.L., Kalwani, M., Garcia-Flores, Y., Luong, M., Devrekanli, A., Xu, J., 2011. miR-146a is a significant brake on autoimmunity, myeloproliferation, and cancer in mice. J. Exp. Med. 208, 1189–1201.
Cheung, K.S., Sposito, N., Stumpf, P.S., Wilson, D.I., Sanchez-Elsner, T., Oreffo, R.O., 2014. MicroRNA-146a regulates human foetal femur derived skeletal stem cell differentiation by down-regulating SMAD2 and SMAD3. PLoS One 9.
Chitwood, D.H., Timmermans, M.C., 2010. Small RNAs are on the move. Nature 467, 415–419.
Cohen-Kfir, E., Artsi, H., Levin, A., Abramowitz, E., Bajayo, A., Gurt, I., Zhong, L., D'Urso, A., Toiber, D., Mostoslavsky, R., 2011. Sirt1 is a regulator of bone mass and a repressor of Sost encoding for sclerostin, a bone formation inhibitor. Endocrinology 152, 4514–4524.
Edwards, J.R., Perrien, D.S., Fleming, N., Nyman, J.S., Ono, K., Connelly, L., Moore, M. M., Lwin, S.T., Yull, F.E., Mundy, G.R., 2013. Silent information regulator (Sir) T1 inhibits NF-κB signaling to maintain normal skeletal remodeling. J. Bone Miner. Res. 28, 960–969.

Gabay, O., Oppenhiemer, H., Meir, H., Zaal, K., Sanchez, C., Dvir-Ginzberg, M., 2012. Increased apoptotic chondrocytes in articular cartilage from adult heterozygous SirT1 mice. Ann. Rheum. Dis. 71, 613–616.
Gabay, O., Sanchez, C., Dvir-Ginzberg, M., Gagarina, V., Zaal, K.J., Song, Y., He, X.H., McBurney, M.W., 2013. Sirtuin 1 enzymatic activity is required for cartilage homeostasis in vivo in a mouse model. Arthritis Rheum. 65, 159–166.
Herranz, D., Muñoz-Martin, M., Cañamero, M., Mulero, F., Martinez-Pastor, B., Fernandez-Capetillo, O., Serrano, M., 2010. Sirt1 improves healthy ageing and protects from metabolic syndrome-associated cancer. Nat. Commun. 1, 1–8.
Hou, J., Wang, P., Lin, L., Liu, X., Ma, F., An, H., Wang, Z., Cao, X., 2009. MicroRNA-146a feedback inhibits RIG-I-dependent Type I IFN production in macrophages by targeting TRAF6, IRAK1, and IRAK2. J. Immunol. 183, 2150–2158.
Iacona, J.R., Lutz, C.S., 2019. miR-146a-5p: expression, regulation, and functions in cancer. Wiley Interdisciplinary Reviews. RNA 10, e1533.
Karrich, J.J., Jachimowski, L.C., Libouban, M., Iyer, A., Brandwijk, K., Taanman-Kueter, E.W., Nagasawa, M., de Jong, E.C., Uittenbogaart, C.H., Blom, B., 2013. MicroRNA-146a regulates survival and maturation of human plasmacytoid dendritic cells. Blood 122, 3001–3009.
Karsenty, G., 2003. The complexities of skeletal biology. Nature 423, 316–318.
Kosik, K.S., 2010. MicroRNAs and cellular phenotypy. Cell 143, 21–26.
Lemieux, M., Yang, X., Jardine, K., He, X., Jacobsen, K., Staines, W., Harper, M., McBurney, M., 2005. The Sirt1 deacetylase modulates the insulin-like growth factor signaling pathway in mammals. Mech. Ageing Dev. 126, 1097–1105.
Li, G., Thabane, L., Papaioannou, A., Ioannidis, G., Levine, M.A., Adachi, J.D., 2017. An overview of osteoporosis and frailty in the elderly. BMC Musculoskelet. Disord. 18, 46.
Magilnick, N., Reyes, E.Y., Wang, W.-L., Vonderfecht, S.L., Gohda, J., J-i, Inoue, Boldin, M.P., 2017. miR-146a–Traf6 regulatory axis controls autoimmunity and myelopoiesis, but is dispensable for hematopoietic stem cell homeostasis and tumor suppression. Proc. Natl. Acad. Sci. 114, E7140–E7149.
Marx, J., 2004. Coming to grips with bone loss. In, American Association for the Advancement of Science.
Nakasa, T., Shibuya, H., Nagata, Y., Niimoto, T., Ochi, M., 2011. The inhibitory effect of microRNA-146a expression on bone destruction in collagen-induced arthritis. Arthritis Rheum. 63, 1582–1590.
Olivieri, F., Lazzarini, R., Recchioni, R., Marcheselli, F., Rippo, M.R., Di Nuzzo, S., Albertini, M.C., Graciotti, L., Babini, L., Mariotti, S., 2013. MiR-146a as marker of senescence-associated pro-inflammatory status in cells involved in vascular remodelling. Age 35, 1157–1172.
Pauley, K.M., Satoh, M., Chan, A.L., Bubb, M.R., Reeves, W.H., Chan, E.K., 2008. Upregulated miR-146a expression in peripheral blood mononuclear cells from rheumatoid arthritis patients. Arthritis Res. Ther. 10, R101.
Qu, B., Cao, J., Zhang, F., Cui, H., Teng, J., Li, J., Liu, Z., Morehouse, C., Jallal, B., Tang, Y., 2015. Type I interferon inhibition of microRNA-146a maturation through up-regulation of monocyte chemotactic protein–induced protein 1 in systemic lupus erythematosus. Arthritis Rheum. 67, 3209–3218.
Rendina-Ruedy, E., Rosen, C.J., 2020. Lipids in the bone marrow: an evolving perspective. Cell Metab. 31, 219–231.
Rigoutsos, I., Furnari, F., 2010. Decoy for microRNAs. Nature 465, 1016–1017.
Saferding, V., Puchner, A., Goncalves-Alves, E., Hofmann, M., Bonelli, M., Brunner, J.S., Sahin, E., Niederreiter, B., Hayer, S., Kiener, H.P., 2017. MicroRNA-146a governs fibroblast activation and joint pathology in arthritis. J. Autoimmun. 82, 74–84.
Saferding, V., Hofmann, M., Brunner, J., Militaru, M., Puchner, A., Hayer, S., Timmen, M., Stange, R., Smolen, J., Blüml, S., 2019. P121/O21 MiR-146A an important key player in bone metabolism. Ann. Rheum. Dis. 78, A54.
Tang, Y., Luo, X., Cui, H., Ni, X., Yuan, M., Guo, Y., Huang, X., Zhou, H., de Vries, N., Tak, P.P., 2009. MicroRNA-146a contributes to abnormal activation of the type I interferon pathway in human lupus by targeting the key signaling proteins. Arthritis Rheum. 60, 1065–1075.
Wu, D., Xi, Q.-Y., Cheng, X., Dong, T., Zhu, X.-T., Shu, G., Wang, L.-N., Jiang, Q.-Y., Zhang, Y.-L., 2016. miR-146a-5p inhibits TNF-α-induced adipogenesis via targeting insulin receptor in primary porcine adipocytes. J. Lipid Res. 57, 1360–1372.
Xie, Q., Wei, W., Ruan, J., Ding, Y., Zhuang, A., Bi, X., Sun, H., Gu, P., Wang, Z., Fan, X., 2017. Effects of miR-146a on the osteogenesis of adipose-derived mesenchymal stem cells and bone regeneration. Sci. Rep. 7, 42840.
Xu, F., Gao, Z., Zhang, J., Rivera, C.A., Yin, J., Weng, J., Ye, J., 2010. Lack of SIRT1 (Mammalian Sirtuin 1) activity leads to liver steatosis in the SIRT1+/− mice: a role of lipid mobilization and inflammation. Endocrinology 151, 2504–2514.
Yoda, M., Kawamata, T., Paroo, Z., Ye, X., Iwasaki, S., Liu, Q., Tomari, Y., 2010. ATP-dependent human RISC assembly pathways. Nat. Struct. Mol. Biol. 17, 17.
Zhang, X., Wang, C., Zhao, J., Xu, J., Geng, Y., Dai, L., Huang, Y., Fu, S.-C., Dai, K., Zhang, X., 2017. miR-146a facilitates osteoarthritis by regulating cartilage homeostasis via targeting Camk2d and Ppp3r2. Cell Death Dis. 8, e2734.
Zhao, J.L., Rao, D.S., Boldin, M.P., Taganov, K.D., O'Connell, R.M., Baltimore, D., 2011. NF-κB dysregulation in microRNA-146a–deficient mice drives the development of myeloid malignancies. Proc. Natl. Acad. Sci. 108, 9184–9189.
Zhao, J., Huang, M., Zhang, X., Xu, J., Hu, G., Zhao, X., Cui, P., Zhang, X., 2019. MiR-146a deletion protects from bone loss in OVX mice by suppressing RANKL/OPG and M-CSF in bone microenvironment. J. Bone Miner. Res. 34, 2149–2161.